Acta Cryst. (1986). A42, 493-501

On the Usefulness of the Concept of the Dispersion Surface Introduced by Professor P. P. Ewald

BY M. J. WHELAN

Department of Metallurgy and Science of Materials, University of Oxford, Parks Road, Oxford OX1 3PH, England

(*Received* 18 *February* 1986; *accepted* 2 *May* 1986)

Abstract

A review is given of the concept of the dispersion surface introduced by Ewald [*Ann. Phys.* (*Leipzig*). (1917), **54**, 519-597] and its importance in the development of the dynamical theory of diffraction. Applications to a few selected areas of importance in the electron diffraction case, such as extinction contours, defect scattering and many-beam effects, are mentioned.

1. Introduction

In the third of Professor Ewald's series of classic papers (Ewald, 1916*a*, *b*; 1917) the subject of crystal optics of X-rays was developed, the first two papers of the series having considered crystal optics of the visible spectrum.* In this paper a very important and useful concept was introduced, namely that of the dispersion surface. This surface is the locus in **k**-space of the wave vectors of crystal wave fields which satisfy the dispersion equations of dynamical self-consistency. It is interesting to note that in Darwin's (1914*a*, *b*) alternative approach to dynamical scattering of X-rays *via* specular-type Bragg reflections from planes, the concept of the dispersion surface was not introduced, although it can be developed by this approach, as is demonstrated by Hirsch, Howie, Nicholson, Pashley & Whelan (1965). Unlike Ewald's papers, which were well illustrated with diagrams, Darwin's papers contained only one diagram, and his disinclination to use diagrams may have been the reason why the concept of the dispersion surface was not discovered by him in 1914.

2. The dispersion surface

This is the surface defining the **k**-vectors of possible self-consistent wave fields propagating with a given frequency in a medium with periodic dielectric properties. For X-rays the radiation is electromagnetic and the medium may be considered as a periodic array of discrete scattering centres (Ewald, 1917) or as a continuous dielectric with periodic polarizability (Laue, 1931). Also, for X-rays it is necessary to consider the two polarizations of the incident wave, and the Bragg angles are not necessarily small. This introduces complications when dealing with certain situations, for example dislocation images in X-ray topography. The author therefore proposes to limit the discussion to the case of electron diffraction, where one deals with a scalar wave function, and where simplifications arise because of the smallness of Bragg angles. Furthermore, for electrons the frequency is easily varied by varying the incident-beam energy. By variation of the relativistic electron mass, one can go from a situation where the wave theory is more appropriate (for light particles) to one where a 'particle channelling' theory is more appropriate (for heavy particles) (Howie, 1967; Chadderton, 1970). The field of electron diffraction is one where the dynamical theory has received much attention in post-war years because of its direct application to the interpretation of transmission electron microscope images of crystalline materials. Necessarily, the treatment given here is brief, and for further details in the electron case reference should be made to Hirsch *et al.* (1965). Applications of the dynamical theory to neutron diffraction are reviewed by Rauch & Petrascheck (1978) and by Klein & Werner (1983).

For electrons the dispersion surface is a surface in **k**-space of constant total energy of the electron, so the dynamical theory of electron diffraction has close similarities with the quantum-mechanical band theory of solids. Except for low-energy electron diffraction, the energies of the primary beam ($\sim 10^4$ to 10^6 eV) are much higher than those encountered in the band theory of solids (~few eV). Thus we are dealing with constant-energy surfaces at large wave-vector separation from the origin of **k**-space, separations of the order of $50g$ or more, where **g** is a low-order reciprocal-lattice vector. Because of the presence of the surface of the crystal (assumed plane) the periodicity is essentially two-dimensional, and the form of the dispersion surface is determined by the

* An interesting account of how much of this work came to fruition while Professor Ewald was an X-ray technician with the German army on the eastern front in the First World War is given by Ewald (1962).

0108-7673/86/060493-09$01.50

two-dimensional (for axial channelling) or the one-dimensional (for planar channelling) band structure for the component of motion of the electron parallel to the surface. In the Laue case the electron beam is incident almost normally on, and is transmitted through, a crystal slice. In a projection approximation the potential along the z direction normal to the slice is smoothed out to give one- or two-dimensionally periodic channels, and the transverse (x, y) motion is determined by the band structure in these channels. The total energy E can be expressed as the sum of the transverse component E_t and the normal component $\hbar^2 k_z^2/2m$ along the channels,

$$E = E_t(\mathbf{k}_t) + \hbar^2 k_z^2/2m. \qquad (2.1)$$

k_z is the component of electron wave vector $\mathbf{k}$ along the channel direction z, while $\mathbf{k}_t$ is the vector component parallel to the surface. m is the relativistic mass of the electron at energy E. $E_t(\mathbf{k}_t)$ gives the transverse energy bands and the relativistic mass enters into the calculation of E_t as well as E_z. For a constant total energy E, if the 'arrow' end of the wave vector $\mathbf{k}(\mathbf{k}_t, k_z)$ is located at the origin of $\mathbf{k}$-space, the 'tail' end lies on one of the branches of the dispersion surface of constant E in (2.1). In the case of electron diffraction the calculation of the shape of the dispersion surface is a problem of solution of Schrödinger's equation for the wave function of the electron in the periodic potential of the crystal. It is well known that the solutions are Bloch functions of the form

$$B^{(i)}(\mathbf{k}, \mathbf{r}) = \sum_g C_g^{(i)}(\mathbf{k}^{(i)}) \exp\{i[\mathbf{k}^{(i)} + \mathbf{g}] \cdot \mathbf{r}\}, \quad (2.2)$$

where $\mathbf{g}$ (and $\mathbf{h}$ below) denote vectors in the reciprocal lattice. The coefficients $C_g^{(i)}$ which depend on $\mathbf{k}^{(i)}$ [particularly on the transverse component of $\mathbf{k}^{(i)}$] are obtained by solution of the dispersion equations

$$\{\mathbf{K}^2 - [\mathbf{k}^{(i)} + \mathbf{g}]^2\} C_g^{(i)} + \sum_{h \neq g} U_{g-h} C_h^{(i)} = 0. \quad (2.3)$$

$\mathbf{K}$ is the wave vector of the incident wave after correction for the mean inner potential ($\mathbf{K}^2 = \boldsymbol{\chi}^2 + U_0$, where $\boldsymbol{\chi}$ is the vacuum wave vector), and the U's are proportional to the Fourier coefficients of the crystal-lattice potential. $U_g = (2me/\hbar^2) V_g$, where m is the relativistic electron mass, V_g is the Fourier coefficient of the lattice potential, and e and $\hbar$ have their usual meaning. The U's are calculable to a good approximation from knowledge of the crystal structure and atomic scattering factors for electrons. In (2.2) it is usual to normalize the C's so that $\sum_g |C_g|^2 = 1$. The equations (2.3) in electron diffraction theory are directly analogous to the dispersion equations obtained by Ewald (1917) in his treatment of the self-consistent wave fields which can exist inside a periodic arrangement of dipole scatterers in the X-ray case.

In general, for a given total energy E, there will be an infinite number of Bloch functions $B^{(i)}$ (not all with real k_z) of the form of (2.2), and an infinite number of dispersion equations (2.3), one for each value of i. In practical computations (2.3) is truncated by limiting the number of equations to a finite number n of $\mathbf{g}$ vectors parallel to the crystal surface. Provided the largest $\mathbf{g}$ is less than the radius of the Ewald sphere, there are n real values of $\mathbf{k}$ corresponding to Bloch waves propagating into the crystal. There are also n further solutions with $\mathbf{k}$ corresponding to Bloch waves propagating backwards. For a parallel-sided plate crystal both types of Bloch waves are required for matching with the incoming and outgoing diffracted waves at the surfaces. Back-scattered waves as well as forward-propagating waves at the entrance surface arise. A formal exact solution may be obtained taking account of all waves (Pendry, 1969; Whelan, 1975), but the usual approximation at high energies neglects the back-scattered waves.

The solution for the wave function $\psi(\mathbf{r})$ inside the crystal is

$$\psi(\mathbf{r}) = \sum_i A^{(i)} B^{(i)}(\mathbf{k}^{(i)}, \mathbf{r}). \qquad (2.4)$$

This is a linear superposition of Bloch waves, one with amplitude $A^{(i)}$ on each of the various branches i of the dispersion surface. The $A^{(i)}$'s are determined by matching the incoming incident plane wave to the wave function (2.4) at the entrance (top) surface of the crystal. The usual boundary conditions apply, *i.e.* the tangential components of wave vectors must be equal, or differ by a surface reciprocal-lattice vector $\mathbf{g}$. Equations (2.2) and (2.4) give the following expression for the various diffracted beams $\mathbf{g}$ in the crystal:

$$\sum_i A^i C_g^{(i)} \exp\{i[\mathbf{k}^{(i)} + \mathbf{g}] \cdot \mathbf{r}\}. \qquad (2.5)$$

These waves must be matched to outgoing plane waves below the exit (bottom) surface of a plate crystal to calculate the amplitudes of various diffracted beams. It is not proposed to go into too much mathematical detail here. The main points are that we must have a knowledge of permissible crystal wave vectors, *i.e.* a knowledge of the dispersion surface. We then select those crystal waves which satisfy the boundary conditions at the top surface and allow them to propagate through the crystal. It is clear from (2.5) that for a given diffracted beam $\mathbf{g}$ there will be beating effects between the various wave vectors $\mathbf{k}^{(i)} + \mathbf{g}$, *i.e.* the amplitude of the beam will oscillate in a complex fashion as it propagates.

The so-called two-beam solution, where only the 0 and $\mathbf{g}$ beams are important in (2.5), can be evaluated analytically for both the Bragg case of diffraction (Darwin, 1914*a*, *b*; Ewald, 1917), where (for high-energy electrons) the Bragg reflecting planes are almost parallel to the crystal surface, and for the Laue case (Ewald, 1917), where (again for high-energy

electrons) the reflecting planes are almost perpendicular to the surface. The theory may also be generalized in the Laue case to take account of more than one Bragg reflection. A formal solution to the n-beam Laue case can be developed using matrix methods for the numerical solution of (2.3). Transmission through a plate crystal can then be formulated using the concept of the scattering matrix, and solutions are now routinely obtained using computer calculations. We mention some results in § 3.3.

To understand the concept of the dispersion surface consider the zero-order approximation to (2.3), where all the Fourier coefficients U_g $(g \neq 0)$ are 'switched off'. Then $[\mathbf{k}^{(i)}+\mathbf{g}]^2 = \mathbf{K}^2$, and this describes a series of 'free-electron' spheres of radius K centred about each of the various reciprocal-lattice points $\mathbf{g}$ parallel to the surface. A few of the intersections of these spheres are shown schematically in Fig. 1(a), and they constitute the zero-order approximation to the many branches of the dispersion surface. Now when the U_g's are gradually switched on, the degeneracy at the intersections of the spheres is removed and a splitting into two branches occurs as shown. In the two-beam approximation only the intersection of the spheres around 0 and $\mathbf{g}$ in Fig. 1(a) is important. In the X-ray case where $\mathbf{g}$ and $\mathbf{K}$ can be of comparable magnitude (large Bragg angles), the situation in the vicinity of the intersection is as shown in Fig. 1(b). Near the intersection the traces of the spheres in the plane of the diagram are approximately straight lines which intersect at twice the Bragg angle at the Brillouin zone boundary. The separation of the two branches of the dispersion surface is much smaller in scale than indicated in Fig. 1(b). For X-rays, order-of-magnitude calculations show that $\Delta k/K \sim 10^{-6}$, so that the splitting of the two branches is extremely small. Thus to a good approximation the important part of the dispersion surface consists of the two branches of a hyperbola with the straight lines as asymptotes. On the other hand, for electrons of energy $\sim 10^5$ eV, $\Delta k/K \sim 10^{-4}$. Furthermore, the radius K of the spheres in Fig. 1(a) is much greater than in the X-ray case, and the splitting of the branches of the dispersion surface at the top intersections is comparable to the distance H in Fig. 1(a). This means that the hyperbolic approximation to the shape of the dispersion surface is, unlike the X-ray case, a poor approximation which becomes poorer for increasing energy and increasing atomic number.

It is to be noted in Fig. 1(a) that, for the one-dimensional (planar channelling) case illustrated, the dispersion surface is periodic with period $\mathbf{g}$ and is a surface of rotation about $\mathbf{g}$. For the two-dimensional (axial channelling) case the periodicity is that of the surface Brillouin zone. Furthermore, only a few of the intersections of the spheres are shown schematically in Fig. 1(a), but if it is borne in mind that the radius K of a sphere may be typically 50 to 200 times g in the energy range 10^5 to 10^6 eV, numerous intersections are possible, as shown in Fig. 9.

3. Some applications in which the dispersion surface plays a leading role

3.1. *The two-beam solution of dynamical theory*

We mention here mainly the Laue case since this has a direct bearing on the interpretation of electron-microscope images of crystals, from which field some illustrative examples will be drawn. The situation is shown in Fig. 1(b). The incident wave vector $\boldsymbol{\chi}$ outside the crystal is represented by **AO**, while **BO** represents the wave vector $\mathbf{K}$ after correction for the mean inner potential. $\mathbf{n}$ is a normal to the crystal surface through A, which intersects the two branches (1, 2) of the dispersion surface to give the required crystal wave vectors. The amplitudes $A^{(1)}$ and $A^{(2)}$of (2.4) can be evaluated in terms of the dimensionless dynamical

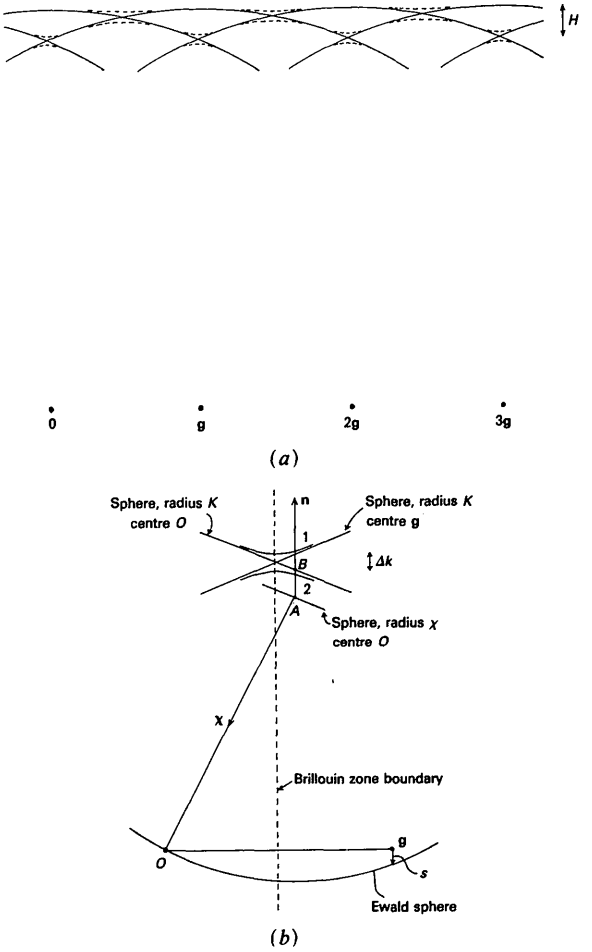

Fig. 1. (a) Schematic dispersion surface for a row of reciprocal-lattice points (planar channelling or systematic reflections). (b) Two-beam dispersion surface. $\boldsymbol{\chi}$ (= **AO**) is the incident vacuum wave vector. $\mathbf{K}$ (= **BO**) is the incident wave vector corrected for the mean inner potential. $\mathbf{n}$ is normal to the crystal surface. The symmetrical Laue case is illustrated.

deviation parameter $w = \xi_g s$. s is the distance of the reciprocal-lattice point from the Ewald sphere (Fig. 1*b*), and ξ_g is the so-called extinction distance for the Bragg reflection **g**. Physically ξ_g is the beat distance of the two waves at the closest separation of the branches of the dispersion surface. ξ_g is calculable from a knowledge of the crystal structure and atomic scattering factors. Typically ξ_g is of the order of a few hundred ångströms for low-order reflections in metals (*e.g.* at 100 keV, for Al, $\xi_{111} \simeq 550$ Å; for Cu, $\xi_{111} \simeq 240$ Å). The amplitudes $A^{(1)}$, $A^{(2)}$ vary along the branches as the point A moves, *i.e.* as the orientation of the incident beam is varied. $A^{(i)}$ tends to unity for those branches asymptotic to the sphere centred at O. At the Brillouin-zone boundary ($s = w = 0$) $A^{(1)} = A^{(2)}$, and waves on both branches are equally excited. Account must also be taken of the variation of $C_0^{(1)}$, $C_g^{(1)}$ and $C_0^{(2)}$, $C_g^{(2)}$ [(2.2)] on each branch.

Assuming an incident wave of unit amplitude, the theory gives the following expressions for the amplitudes φ_0 and φ_g of direct and diffracted waves transmitted through a plate crystal of thickness t in the symmetrical Laue case.

$$\varphi_0 = \cos \pi t\bar{s} - [iw/(1+w^2)^{1/2}] \sin \pi t\bar{s} \quad (3.1)$$

$$\varphi_g = (i\pi/\xi_g)(\sin \pi t\bar{s}/\pi\bar{s}) \quad (3.2)$$

where $\bar{s}^2 = s^2 + \xi_g^{-2}$.

The expression (3.2) for the diffracted-beam amplitude is formally the same as that derived from kinematical scattering theory except that s of kinematical theory is replaced by $\bar{s}$. Equation (3.2) is a sort of modified shape transform.

For a given crystal orientation, (3.1) and (3.2) predict that the direct and diffracted beams oscillate with depth, the *Pendellösung* solution, where the current is scattered back and forth between direct and diffracted beams. At the Bragg reflecting position ($s = 0$) the depth periodicity is equal to the extinction distance ξ_g. Fig. 2 shows examples of such 'thickness extinction contours' in a thin foil of Cu–7wt% Al alloy observed by transmission of electrons in an electron microscope. The image is a bright-field one, taken with an aperture excluding the diffracted beam. Also visible are images of dislocation lines threading the foil. Many of the lines appear to zig-zag, but care must be taken not to interpret such effects as a true zig-zag configuration of the dislocation line. The dislocation line itself is probably straight. The zig-zag effect arises because of the interaction of the dislocation displacement field with the *Pendellösung* periodicity of the wave field, *i.e.* the depth periodicity of the zig-zag is determined by ξ_g (Howie & Whelan, 1962).

A crystal foil which bends over the field of view so that a region is tilted through the Bragg position shows 'bend extinction contours'. Fig. 3 is an example of a bend extinction contour in aluminium foil where the thickness t varies from top to bottom. In the thin regions to the left, subsidiary oscillations are visible which correspond loosely to the oscillations with s of the shape-transform function of (3.2). In practice only a qualitative interpretation is possible using two-beam theory. The actual bend contour in Fig. 3 corresponds mainly to a pair of Bragg reflections from opposite sides of {111} planes. The detailed interpretation requires n-beam theory applied to the planar channelling case, *i.e.* to the 'systematic' reflections occurring for a prominent row of the reciprocal lattice. Nevertheless, the two-beam theory gives a good qualitative understanding (Hashimoto, Howie & Whelan, 1962).

At this point attention should be drawn to the decreasing visibility of thickness fringes in Fig. 2 and subsidiary bend fringes in Fig. 3 in the thicker regions of the specimen. In Fig. 2, for example, only about four dark fringes are clearly visible. This is the electron counterpart of the well known Borrmann (1941) effect observed in X-ray diffraction and explained by Laue (1949). At the Bragg position with two-beam theory, the current distribution associated with branch 1 of the dispersion surface in Fig. 1(*b*) has antinodes on the Bragg planes, whereas that on branch 2 has nodes on the Bragg planes. Now if absorption processes occur which are localized near the atomic sites, it is clear that the branch-1 wave will be absorbed more than the branch-2 wave. Hence in the thick regions of Fig. 2 the fringes (which are essentially due to beating between the two waves) fade out, and the transmission observed is essentially due to wave 2. Furthermore, in Fig. 3 the good transmission in the thick regions Y on either side of the dark contour corresponds to the direct-beam transmission peak which occurs for slightly positive values

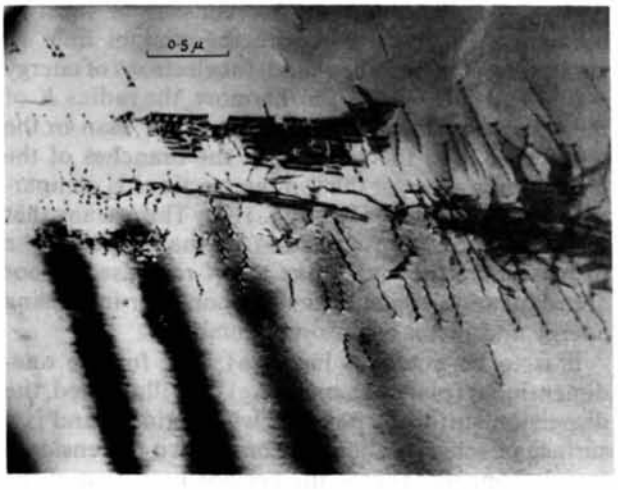

Fig. 2. Thickness extinction contours and dislocation images in a bright-field transmission electron microscope image of a wedge crystal of Cu–7wt% Al alloy. 100 kV electrons. After Howie & Whelan (1962).

of w $(=\xi_g s)$ for the reflections 111 and $\bar{1}\bar{1}\bar{1}$ respectively. It is true to say that the attainment of good transmission in relatively thick crystalline specimens owes much to the presence of the Borrmann effect, *i.e.* thicker specimens of crystalline material are able to be examined than if the material were microcrystalline or amorphous.

The mechanisms of the absorption processes differ in the X-ray and electron cases. For X-rays photoelectric absorption is the main mechanism, while for electron-microscope images the main mechanism is large-angle diffuse scattering due to phonon excitation outside the acceptance angle of the objective lens. However, both X-ray and electron cases can be described by the same type of phenomenological theory whereby complex Fourier coefficients of the polarizability or of the lattice potential are introduced.

The *Pendellösung* phenomenon in the Laue case is most strikingly demonstrated by the images of stacking faults observed in transmission electron microscopy. A stacking fault is a planar defect at which an abrupt displacement **R** (not equal to a lattice vector) occurs, which divides the crystal into two parts with a relative phase difference $2\pi\mathbf{g}.\mathbf{R}$ between waves diffracted into the Bragg reflection **g** from either part. Figs. 4(*a*), (*b*) show an example of such a fault in Cu–7wt% Al alloy running through the foil at an angle so that the edges P and Q correspond to the intersections with top and bottom surfaces respectively. We have in effect two overlapping wedge crystals out of phase with each other. The fringes observed arise because of the disruption of the *Pendellösung* oscillations at the plane of the fault. Fig. 4(*a*) corresponds to the direct beam (bright-field image) while Fig. 4(*b*) is the diffracted beam (dark-field image). It is noticed that the bright-field image is symmetrical with bright fringes on opposite sides, whereas the dark-field image is asymmetrical with edges P and Q terminating in light and dark fringes respectively. It is also seen that the fringes are less visible near the centre of the fault image. The theory of stacking-fault fringes was worked out by Whelan & Hirsch (1957*a*, *b*) and (for the case of absorption) by Hashimoto *et al.* (1962), and for details these papers should be consulted. The two-beam theory including absorption explains the observations quite well, as Fig. 5 shows. The full curve is the bright-field (symmetric) image while the broken curve is the dark-field (asymmetric) image. The calculations predict the reduced visibility of the central fringes observed experimentally. The physical explanation of these effects in terms of the behaviour of various waves excited on the two branches of the dispersion surface has been discussed by Hashimoto *et al.* (1962). For a more detailed review the reader should consult Hirsch *et al.* (1965) or Whelan (1975).

Finally, some mention should be made of the two-beam solution in the Bragg case, since historically this was the first case studied by Darwin (1914*b*) for X-ray diffraction. As mentioned in § 1 Darwin obtained his solution mathematically without resort to diagrams. Darwin's 'rocking curve' in the Bragg case is shown in Fig. 6 for the case of no Borrmann absorption. The main feature is a region of total reflection of width $2\xi_g^{-1}$ in the s parameter (Fig. 1*b*). The displacement of the centre of this curve away from $s=0$ is due to the mean refractive index. Ewald (1917) obtained a similar curve with total reflection over the same range and differing from Darwin's curve only in the tails ($|w|=\xi_g|s>1$), a difference which arose through different assumptions concerning absorption.

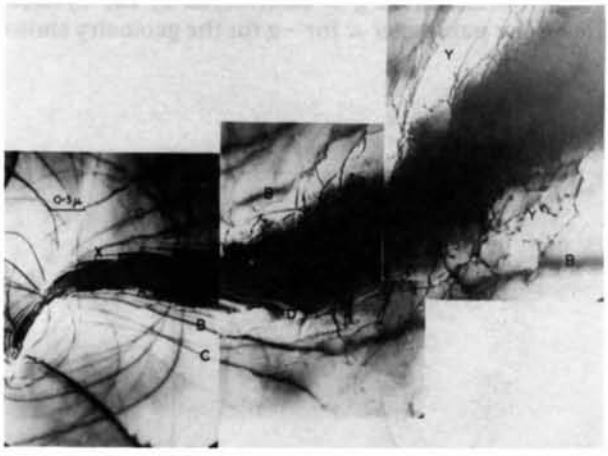

Fig. 3. A bend extinction contour in a bright-field transmission electron microscope image of a region of aluminium foil of varying thickness. 100 kV electrons. *A*: principal contour corresponding to 111 and $\bar{1}\bar{1}\bar{1}$ reflections in thin region ($t\sim 1{\cdot}5\xi_g$). *Y*: thick region. After Hashimoto, Howie & Whelan (1962).

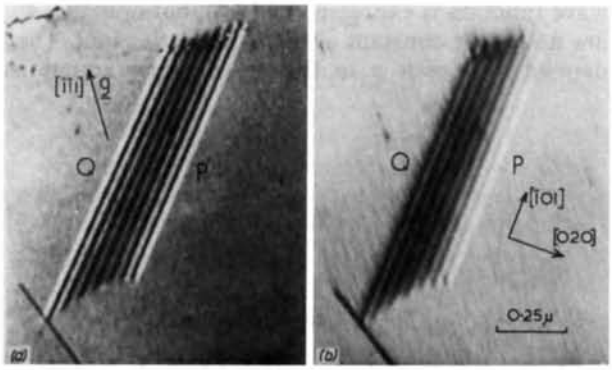

Fig. 4. (*a*) Bright-field and (*b*) dark-field transmission electron microscope images of a stacking fault in Cu–7wt% Al alloy. 100 kV electrons. Note the symmetry and asymmetry of the fringes in bright and dark field respectively. After Hashimoto, Howie & Whelan (1962).

However, the main feature of Darwin's solution can be understood in terms of the dispersion surface of Fig. 1(*b*). In the symmetric Bragg case, the normal **n** to the crystal surface is at right angles to that shown in Fig. 1(*b*). Therefore, as the incident wave point A moves along the sphere of radius χ about O, it is clear that there will be a limited region where no real intersection of **n** with the dispersion surface occurs. In this region the wave vector component along **n** is complex, and the imaginary part gives rise to an evanescent crystal wave which carries no net current. Thus the incident wave is completely reflected. If Borrmann absorption occurs the shape of the rocking curve is modified [for a review see James (1948)].

3.2. *Defect scattering*

In both X-ray diffraction and electron diffraction the presence of defects such as stacking faults and dislocation lines perturbs the crystal wave field, and as a result such defects are made visible on X-ray topographs or electron micrographs. Examples of dislocation and fault images in the electron case have already been given (Figs. 2 and 4). For electron diffraction the theoretical treatment is in many respects simpler than the X-ray case because of the smallness of Bragg angles and the absence of polarization complications. Furthermore, in the electron case the incident-beam divergence is usually less than the angular range of reflection of the crystal so that a plane-wave theory is sufficient. For X-rays the opposite is usually the case, and integration over beam divergence is required. The smallness of Bragg angles implies that the electrons can be considered to propagate in a narrow column (the so-called 'column approximation'), and the problem can be reduced to one of overlapping slices which are shifted by the defect displacement field.

The effect of a defect can be described in terms of interbranch scattering of Bloch waves between various branches of the dispersion surface. The crystal wave function is expressed by (2.4), but now the $A^{(i)}$ are no longer constant as for a perfect crystal. They depend on depth z in the crystal. The equations describing the process are

$$\mathrm{d}A^{(i)}/\mathrm{d}z = 2\pi i \sum_i \sum_g (\mathbf{g}\,.\,\mathrm{d}\mathbf{R}/\mathrm{d}z) C_g^{*(i)} C_g^{(j)} \times \exp\{2\pi i[k_z^{(j)} - k_z^{(i)}]z\} A^{(j)}. \quad (3.3)$$

These are linear equations describing a sort of redistribution of amplitude between the various branches of the dispersion surface, a process which has been referred to as 'tie-point jumping' in the X-ray case following the terminology for a point on the dispersion surface introduced by Professor Ewald. Equation (3.3) shows that it is the derivative of the displacement field (*i.e.* the local tilt of lattice planes) which causes the redistribution of amplitude.

Equations more general than (3.3), not relying on the column approximation and taking account of lateral variations of the displacement field, were formulated by Takagi (1962) for electrons and by Taupin (1964) for X-rays. The approach used by Takagi and Taupin considered the effect of the defect displacement field on the total wave amplitudes. Howie & Whelan (1961*b*) formulated a similar theory for electron scattering in the two-beam case using the column approximation following the approach used by Darwin (1914*a*, *b*).

3.3. *n-beam effects*

As mentioned in § 2, calculations of n-beam diffraction in the Laue case using computer matrix methods are now routine. The importance of n-beam effects in electron diffraction can be understood by considering the case of 'systematic' reflections as shown in Fig. 7. Owing to the large radius of curvature of the Ewald sphere, if the reciprocal-lattice point **g** is on the sphere, then $-\mathbf{g}$ is inevitably close to the sphere. Whether or not $-\mathbf{g}$ perturbs appreciably the two-beam result for reflection **g** is determined by the dynamic deviation parameter w for $-\mathbf{g}$ for the geometry shown

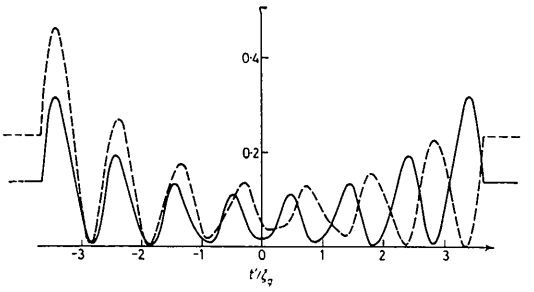

Fig. 5. Computed profiles of the stacking fault images of Fig. 4. After Hirsch, Howie, Nicholson, Pashley & Whelan (1965).

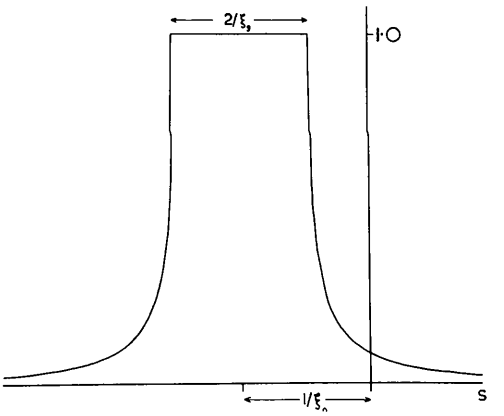

Fig. 6. Rocking curve of a crystal in the Bragg case of diffraction. The ordinate is the reflected intensity.

in Fig. 7. A simple calculation shows that $w = g^2/U_g$. If this parameter is less than unity, the reflection $-\mathbf{g}$ is strong and n-beam effects become important. Now U_g at a given energy increases with atomic number, and also for a given element it increases with energy in proportion to the relativistic electron mass. For a light element such as aluminium, this criterion shows that two-beam theory is reasonably good at 100 keV but is less so at 1 MeV. However, for a heavy element such as gold the two-beam theory is poor even at 100 keV.

Fig. 8(a) shows the first four branches of the dispersion surface for aluminium at 100 keV calculated for seven systematic reflections (Howie & Whelan, 1961a). It is clear that even for this light element branches 1 and 2 of the dispersion surface are far from being parabolic in shape. Nevertheless, waves on branches 1 and 2 predominate when $\mathbf{g}$ is nearly satisfied making the two-beam theory a reasonable approximation. Fig. 8(b) shows the variation of absorption coefficient for each branch, with increased and reduced absorption for branches 1 and 2 respectively at $k_x/g = 0{\cdot}5$ (Bragg position) as expected from the Borrmann effect.

Calculations for heavy elements at higher energies show marked deviations in the shapes of the first two branches of the dispersion surface from that expected by two-beam theory. Fig. 9 (Humphreys & Lally, 1970) shows several branches of the dispersion surface for gold at 500 keV and 1 MeV. A considerable flattening of the first two branches is evident, with a similar tendency for the third branch. Furthermore, if the symmetries of the Bloch functions for branches 1 and 2 at $k_x/g = 0, 0{\cdot}5$ are examined, it is found that the functions are either symmetric (S) or antisymmetric (A) with respect to the positions of the atomic Bragg planes. The symmetry and antisymmetry simply correspond to Bloch waves with current antinodes or nodes at the atomic planes as in the explanation of the Borrmann effect. For branches 3 and higher, the symmetries at $k_x/g = 0$ and $0{\cdot}5$ may be different (*e.g.* see branches 3, 5, 6 at 500 keV).

Now, as discussed in § 2, the form of the dispersion surface is determined by the transverse motion of the electron in the channels as per (2.1). If the potential $U(x)$ of the channel becomes very deep, as happens when the Fourier coefficients U_g increase at high energy in proportion to the relativistic electron mass, one approaches a situation where the barriers between the channels are impenetrable. In this limit the lateral motion of the electron is determined by the transverse states in a single channel, the lowest state corresponding to the top branch of the dispersion surface. Furthermore, as in the tight-binding approximation of band theory, for a periodic array of channels with impenetrable barriers the energy will be independent of the lateral-band wave vector k_x. This accounts for the tendency mentioned above for the upper branches of the dispersion surface to become flatter at high energies. The lowest state for a symmetric well is symmetric, and the higher states alternate with antisymmetric or symmetric wave functions. Thus the symmetries of the first two branches in Fig. 9 are understood in terms of this model (Howie, 1967). Branches 3, 4, 5 *etc.* in Fig. 9 correspond to states of lateral motion that are fairly free and hence the wavefunction symmetry can vary across the branches. However, with increasing electron-beam energy further states become bound in the channels. For an isolated one-dimensional square potential well of depth U and width $\frac{1}{2}d$, the condition for binding a second state is well known from elementary quantum

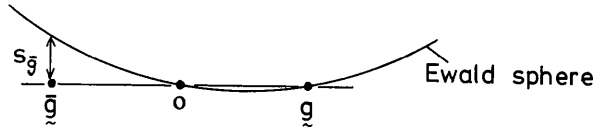

Fig. 7. Ewald sphere construction for a systematic row of reflections.

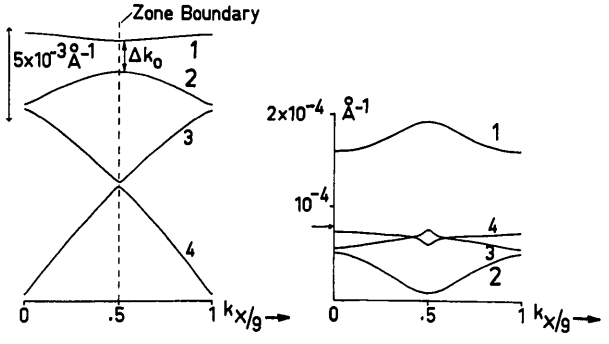

Fig. 8. (a) Dispersion surface of aluminium calculated for seven-beam systematic {111} reflections, 100 kV electrons. (b) Absorption coefficients on the branches of the dispersion surface. After Howie & Whelan (1961a).

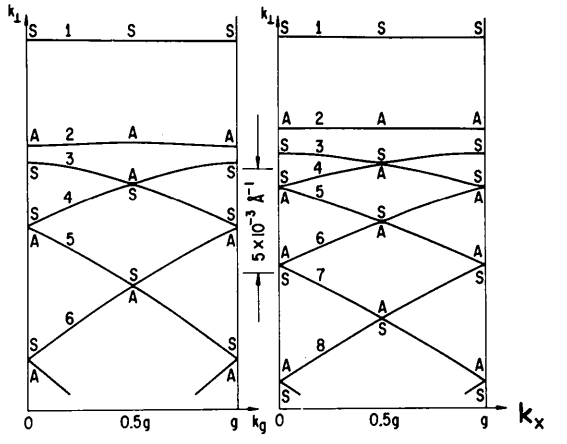

(a) 500 keV (b) 1 MeV

Fig. 9. Dispersion surfaces for gold 111 systematic reflections at 500 keV and 1 MeV. After Humphreys & Lally (1970).

mechanics to be $d^2U > 1$. For a periodic arrangement of such wells with spacing d, a similar criterion is expected to hold, except that, due to tunnelling between wells, the transition between bound and unbound states will not be so sharp. Since $d = g^{-1}$ and $U \sim U_g$, we see that the criterion $d^2U > 1$ is equivalent to the criterion $g^2/U_g < 1$ mentioned above for the onset of n-beam diffraction effects. Thus there is a subtle connection ['correspondence principle' (Chadderton, 1970)] between the onset of n-beam diffraction effects in a wave treatment and the binding of a particle in crystal channels in a quantum treatment.

When further states become bound in the channels, symmetry changes of the Bloch wave functions occur at $k_x/g = 0$ or 0·5 on dispersion surfaces like Fig. 9. For example, a symmetry change at $k_x/g = 0{\cdot}5$, 1·5 *etc.* occurs for branches 3 and 4 between 500 keV and 1 MeV in Fig. 9. When such a symmetry change occurs, the two branches of the dispersion surface come together and touch each other. The voltage at which this occurs is known as the critical voltage V_c for a corresponding Bragg reflection. The touching of branches 3 and 4 in Fig. 9 at $k_x/g = 0{\cdot}5$ *etc.* occurs at V_c for the $3g$ Bragg reflection. There is a critical voltage below 500 keV for gold where branches 2 and 3 touch and change symmetry at $k_x/g = 0$, 1 *etc.* This is the critical voltage for the $2g$ Bragg reflection.

At a critical voltage, the intensity of a corresponding second- (or higher-) order Bragg reflection becomes very weak. The physical reason for this is that the waves on the two touching branches are the principal contributions to the diffracted beam in question. At the top surface of the crystal these waves must very nearly cancel each other since the total diffracted amplitude must vanish at this surface. However, if the branches are touching, effective cancellation must occur at any depth in the crystal since no relative phase difference due to propagation occurs between the two principal waves. Thus critical voltages can be determined in a high-voltage electron microscope of variable beam energy by observing the vanishing of corresponding reflections.

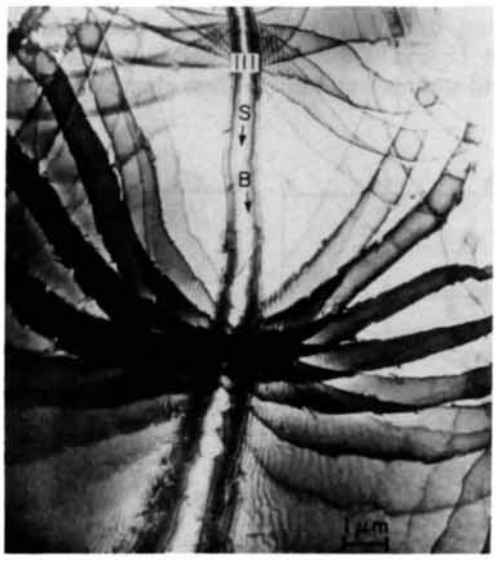

Fig. 10. Bright-field transmission electron micrograph taken with 1 MV electrons of gold showing bend contours around a 123 pole. The symmetry and 111 Bragg positions are marked *S* and *B*. After Humphreys & Lally (1970).

The critical voltage effect was discovered by Nagata & Fukuhara (1967), Uyeda (1968) and by Watenabe, Uyeda & Fukuhara (1968), and it has been used to determine accurate values of low-order Fourier coefficients of the potential (Watenabe, Uyeda & Kogiso, 1968; Thomas, Shirley, Lally & Fisher, 1974; Hewat & Humphreys, 1974). From such accurate measurements applications can be made to problems such as ordering in alloys (Shirley & Fisher, 1979) and the estimation of electron redistribution due to bonding in solids (Smart & Humphreys, 1978).

Finally, we mention the effect of n-beam diffraction on bend extinction contours, and its relevance to penetration at high energies. It was mentioned in § 3.1 with reference to Fig. 3 that for the 111 reflection of aluminium at 100 keV the orientation for good penetration is slightly positive of the {111} Bragg position on either side of the dark contour. However, this is not necessarily the case at high energies where waves on other branches of the dispersion surface can become important. Fig. 10 (Humphreys & Lally, 1970) shows that in gold at 1 MeV the {111} bend contour has a transmission peak at its centre *S*, the symmetry position where the electron is moving exactly parallel to the Bragg planes. This arises because of an increased excitation of the Bloch wave on branch 3 of the dispersion surface, which has a relatively low absorption (Howie, 1966; Humphreys & Lally, 1970). The orientation for optimum penetration can therefore vary at high energies, particularly for heavier elements. These and other factors relevant to the optimum voltage for ultra-high-voltage electron microscopy have been considered by Humphreys (1972).

4. Concluding remark

From what has been mentioned in this review it is clear that the concept of the dispersion surface introduced by Professor Ewald has led to a considerable enhancement of our understanding of many effects arising through dynamical diffraction in both the X-ray and electron cases.

References

BORRMANN, G. (1941). *Phys. Z.* **42**, 157–162.
CHADDERTON, L. T. (1970). *J. Appl. Cryst.* **3**, 429–465.
DARWIN, C. G. (1914*a*). *Philos. Mag.* **27**, 315–333.

DARWIN, C. G. (1914*b*). *Philos. Mag.* **27**, 675-690.
EWALD, P. P. (1916*a*). *Ann. Phys. (Leipzig)*, **49**, 1-38.
EWALD, P. P. (1916*b*). *Ann. Phys. (Leipzig)*, **49**, 117-143.
EWALD, P. P. (1917). *Ann. Phys. (Leipzig)*, **54**, 519-597.
EWALD, P. P. (1962). *J. Phys. Soc. Jpn*, **17**, Supplement B-II, 48-52.
HASHIMOTO, H., HOWIE, A. & WHELAN, M. J. (1962). *Proc. R. Soc. London Ser. A*, **269**, 80-103.
HEWAT, E. A. & HUMPHREYS, C. J. (1974). *High Voltage Electron Microscopy*, edited by P. R. SWANN, C. J. HUMPHREYS & M. J. GORINGE, pp. 52-56. London and New York: Academic Press.
HIRSCH, P. B., HOWIE, A., NICHOLSON, R. B., PASHLEY, D. W. & WHELAN, M. J. (1965). *Electron Microscopy of Thin Crystals*. London: Butterworths.
HOWIE, A. (1966). *Philos. Mag.* **14**, 223-237.
HOWIE, A. (1967). *Proc. Int. Conf. Solid State Physics Research with Accelerators*, Brookhaven National Laboratory 50083 (C-52), pp. 15-29. Washington: Clearing House for Federal Scientific and Technical Information.
HOWIE, A. & WHELAN, M. J. (1961*a*). *Proc. Eur. Regional Conf. on Electron Microscopy (Delft*, 1960), Vol. 1, 181-185. Delft: de Nederlandse Vereniging voor Electronenmicroscopie.
HOWIE, A. & WHELAN, M. J. (1961*b*). *Proc. R. Soc. London Ser. A*, **263**, 217-237.
HOWIE, A. & WHELAN, M. J. (1962). *Proc. R. Soc. London Ser. A*, **267**, 206-230.
HUMPHREYS, C. J. (1972). *Philos. Mag.* **25**, 1459-1472.
HUMPHREYS, C. J. & LALLY, J. S. (1970). *J. Appl. Phys.* **41**, 232-235.
JAMES, R. W. (1948). *The Optical Principles of the Diffraction of X-rays*. London: Bell.
KLEIN, A. G. & WERNER, S. A. (1983). *Rep. Prog. Phys.* **46**, 259-335.
LAUE, M. VON (1931). *Ergeb. Exakten Naturwiss.* **10**, 133-158.
LAUE, M. VON (1949). *Acta Cryst.* **2**, 106-113.
NAGATA, F. & FUKUHARA, A. (1967). *Jpn. J. Appl. Phys.* **6**, 1233-1235.
PENDRY, J. B. (1969). *J. Phys. C*, **2**, 2273-2282.
RAUCH, H. & PETRASCHECK, D. (1978). *Topics in Current Physics*. Vol. 6: *Neutron Diffraction*, Ch. 9, pp. 303-351. Berlin, Heidelberg: Springer.
SHIRLEY, C. G. & FISHER, R. M. (1979). *Philos. Mag.* **A39**, 91-117.
SMART, D. J. & HUMPHREYS, C. J. (1978). *Electron Diffraction 1927-1977. Inst. Phys. Conf. Ser.* No. 41, pp. 145-149. London: The Institute of Physics.
TAKAGI, S. (1962). *Acta Cryst.* **15**, 1311-1312.
TAUPIN, D. (1964). *Bull. Soc. Fr. Minéral. Cristallogr.* **87**, 469-511.
THOMAS, L. E., SHIRLEY, C. G., LALLY, J. S. & FISHER, R. M. (1974). *High Voltage Electron Microscopy*, edited by P. R. SWANN, C. J. HUMPHREYS & M. J. GORINGE, pp. 38-47. London and New York: Academic Press.
UYEDA, R. (1968). *Acta Cryst.* **A24**, 175-181.
WATENABE, D., UYEDA, R. & FUKUHARA, A. (1968). *Acta Cryst.* **A24**, 580-581.
WATENABE, D., UYEDA, R. & KOGISO, M. (1968). *Acta Cryst.* **A24**, 249-250.
WHELAN, M. J. (1975). *Advances in Electronics and Electron Physics*, Vol. 39, edited by L. MARTON, pp. 1-72. New York: Academic Press.
WHELAN, M. J. & HIRSCH, P. B. (1957*a*). *Philos. Mag.* **2**, 1121-1142.
WHELAN, M. J. & HIRSCH, P. B. (1957*b*). *Philos. Mag.* **2**, 1303-1324.

Acta Cryst. (1986). A**42**, 501-510

Observations of Borrmann–Lehmann Interference Patterns with Synchrotron Radiation

BY A. R. LANG AND G. KOWALSKI*

H. H. Wills Physics Laboratory, University of Bristol, Tyndall Avenue, Bristol BS8 1TL, England

A. P. W. MAKEPEACE

Department of Physiology, School of Medicine, University of Bristol, Bristol BS8 1TD, England

AND M. MOORE

Department of Physics, Royal Holloway and Bedford New College, Egham Hill, Egham, Surrey TW20 0EX, England

(*Received* 7 *February* 1986; *accepted* 2 *May* 1986)

Abstract

The intrabranch interference effects expected under Laue-Bragg diffraction conditions [Saka, Katagawa & Kato (1972). *Acta Cryst.* A**28**, 102-113, 113-120] and first studied experimentally under high-absorption conditions by Borrmann & Lehmann [*Crystallography and Crystal Perfection* (1963), edited by G. N. Ramachandran, pp. 101-108. London and New York: Academic Press] have been investigated in the moderate ($\mu_0 t = 1{\cdot}6$) and low ($\mu_0 t = 0{\cdot}47$) absorption cases with Cu $K\alpha_1$ and with synchrotron radiation of wavelengths 1·5 and 1·0 Å. Borrmann-Lehmann fringe patterns have been recorded with σ-mode and π-mode polarizations alone, utilizing the linearly polarized nature of synchrotron radiation. Specimens of natural diamonds possessing faces polished parallel to {100} and {110} were studied. The 220 reflection was recorded with the Laue entrance

* On leave from Institute of Experimental Physics, University of Warsaw, Poland.

0108-7673/86/060501-10$01.50